(above approximately one-fourth the Debye temperature) $f_{\alpha\beta\gamma}$ (which depends on the interatomic potential) is linear in temperature. If one defines

$$g_{\alpha\beta\gamma}=\frac{f_{\alpha\beta\gamma}(T,r)-f_{\alpha\beta\gamma}(T_0,r_0)}{T-T_0}, \quad \text{(A6)}$$

one can obtain a temperature coefficient for the third-order elastic constants

$$C_{\alpha\beta\gamma}(T,r)=C_{\alpha\beta\gamma}(T_0r_0)+A_{\alpha\beta\gamma}\times(T-T_0), \quad \text{(A7)}$$

where

$$A_{\alpha\beta\gamma}=K\frac{\partial}{\partial r}C_{\alpha\beta\gamma}{}^{\Phi}(r)\Big|_{r=r_0}+\frac{g_{\alpha\beta\gamma}}{V_0}. \quad \text{(A8)}$$

In summary, $C_{\alpha\beta\gamma}{}^{\Phi}$ and $g_{\alpha\beta\gamma}$ are independent of temperature by definition. Thus, Eq. (A7) predicts that the third-order constants are linear functions of temperature (above approximately $\frac{1}{4}\Theta$). The slope of a plot of the constants as a function of temperature is the coefficient $A_{\alpha\beta\gamma}$. Future detailed comparison of measured values of this coefficient and the theoretical value as determined from the calculations indicated in Eq. (A7) could conceivably yield important information about interatomic forces.

PHYSICAL REVIEW B VOLUME 1, NUMBER 8 15 APRIL 1970

Paramagnetic *Ni*Cu Alloys: Electronic Density of States in the Coherent-Potential Approximation*

S. KIRKPATRICK,† B. VELICKÝ,‡ AND H. EHRENREICH
Division of Engineering and Applied Physics, Harvard University, Cambridge, Massachusetts 02138
(Received 23 October 1969)

The coherent-potential approximation (CPA) is extended to study general band shapes and systems having orbital degeneracy. This permits its application to realistic systems, in particular the *Ni*Cu alloys. The effects of alloying on a highly asymmetric model density of states characteristic of some of the features of the density of states in fcc transition metals are considered in detail. A model Hamiltonian for paramagnetic *Ni*Cu is constructed using a basis of orthogonalized plane waves and tight-binding *d* functions. Orbital degeneracy and hybridization are treated as in paramagnetic Ni. Effects of alloying are assumed to be restricted to the diagonal elemensts of the *d-d* block. The model is applicable to the Ni-rich alloys, as is the approximation used to obtain simple solutions of the full CPA equations. The results are consistent with recent photoemission data on *Ni*Cu, and with the "minimum polarity" hypothesis used by Lang and Ehrenreich. They are incompatible with the rigid-band model because the scattering potential of the random alloy is strong compared to the peak widths. Rather than a rigid shift of the density of states, the calculated concentration dependence shows that the main peaks remain stationary while changing magnitude and shape. Decomposition of the total density of states into Ni and Cu contributions confirms that, for the expected position of the Fermi level, the *d* holes are located primarily on Ni sites.

I. INTRODUCTION

IN this paper the electronic density of states and other one-electron properties of the *Ni*Cu alloys above their Curie temperatures are studied within the coherent-potential approximation (CPA).[1] The work reported is the first attempt to apply the CPA to a real alloy system.

The CPA, introduced by Soven[1] for the study of electrons in a substitutional alloy, and earlier by Taylor[2] for the formally similar phonon case, has been studied in detail in several recent papers.[3–5]

The CPA results from the self-consistent solution of the usual multiple-scattering version[6] of the Schrödinger equation, within a single-site approximation,[4] in which the properties of all sites but one are averaged over, and that one is treated exactly. It has therefore been found useful in the description of short-ranged scattering in the alloy. The principal advantage of the CPA over other simple approximations results from its self-consistency; the CPA extrapolates away from the limits of low concentration and weak scattering in a physically reasonable way. Effects due to details of the possible local surroundings of a site, are of course averaged over in this approximation. However, we are not interested, in the calculations to be reported, in such refinements as "tails"[7] of localized states.

The idealized model treated in VKE based on a nondegenerate tight-binding band is far removed from a real alloy, but *Ni*Cu proves to be a good candidate for treatment by an alloy theory not very much more

* Supported in part by Grant No. GP-8019 of the National Science Foundation and the Advanced Research Projects Agency.
† Present address: The James Franck Institute, the University of Chicago, Chicago, Ill. 60637.
‡ Present address: Institute of Solid State Physics, Czechoslovak Academy of Sciences, Prague.
[1] P. Soven, Phys. Rev. **156**, 809 (1967).
[2] D. W. Taylor, Phys. Rev. **156**, 1017 (1967).
[3] Y. Onodera and Y. Toyozawa, J. Phys. Soc. Japan **24**, 341 (1968).
[4] B. Velický, S. Kirkpatrick, and H. Ehrenreich, Phys. Rev. **175**, 747 (1968), henceforth abbreviated VKE.
[5] P. Soven, Phys. Rev. **178**, 1136 (1969).
[6] M. Lax, Rev. Mod. Phys. **23**, 287 (1951).
[7] I. M. Lifshitz, Usp. Fiz. Nauk **83**, 617 (1964) [Soviet Phys.—Usp. **7**, 549 (1965)].

sophisticated than that of VKE. It exists in the same fcc form for all concentrations with no ordered phases. The lattice constant changes by only $2\frac{1}{2}\%$ between pure Ni and pure Cu.[8] There is evidence for clustering of like atoms in a single *Ni*Cu sample of roughly equal concentrations,[9] but the clustering observed is slight and short-ranged. Far beyond the scope of this study is recent observation of the magnetic properties of the *Ni*Cu alloys at large Cu concentrations,[10] which suggest that the local environment has a strong influence on the magnetic susceptibility of an individual Ni atom in the alloy. Since we shall seek only the average electronic properties at low Cu concentrations, it will be sufficient to picture *Ni*Cu as an ideal binary substitutional alloy.

The electronic band structures of pure Ni [11] and pure Cu [12] are well known. Comparison of these band structures reveals that the only substantial differences lie in the *d* bands. They differ enough to preclude use of perturbation theory or the rigid-band model[13] in the alloy. However, since they have basically a tight-binding character, the alloy is suitable for treatment within the single-site approximtion.

*Ni*Cu therefore has many of the properties of the single-band substitutional alloy treated in VKE. It differs, however, in that hybridization with the *s* band occurs, the *d* bands are fivefold degenerate, and the shape of each band, in contrast to the simple model band used in VKE, is quite complex. The third of these differences is studied, within the nondegenerate band scheme, in Sec. II, by introducing a highly asymmetric "steeple" state density with a sharp peak to represent the presence of critical points. It is found that the asymmetry of the band introduces no complications, but that the width of the peak becomes an important new parameter of the problem. Only when the strength of the random scattering is much less than this width is the weak-scattering limit attained. This observation has immediate relevance to Ni and Cu, for the density of states in each has characteristics found in the "steeple" model.

Hybridization and orbital degeneracy are added to the model in Secs. III and IV. In Sec. III, a model Hamiltonian, based on the *s-d* interpolation schemes of Hodges *et al.*[14] and Mueller,[15] is constructed. We start with pure Ni, in order to describe the Ni-rich alloys, and show that the most important effect of alloying is to shift down the atomic *d* levels at Cu sites. The size of the shift is estimated by comparing the Ni and Cu band structures, as well as by consideration of the energy levels of the Hartree-Fock potentials appropriate to the respective band calculations. The results of the two procedures agree. This gives rise to a short-ranged scattering which the CPA can, in principle, treat.

The CPA equations for the properties of the averaged alloy, derived in Sec. IV, are simple in form, but difficult to solve. The effective Hamiltonian describing the averaged system contains a scattering contribution of two components, of t_{2g} and e_g local symmetry. These satisfy a system of coupled equations analogous to the CPA equations for the single band. It is shown in Sec. IV that the equations can be decoupled in the limit of the Ni-rich alloys, even in the presence of degeneracy and hybridization.

In Sec. V we calculate an alloy state density for *Ni*Cu, using only the density of states as input. Results are given for several values of the concentration. Partial densities of states from Ni or Cu sites may also be obtained in the CPA, and are studied in this section to estimate the amount of charge transfer in the alloy, and the consistency of our initial assumption of neutral configurations for each type of atom.

Finally, we compare the total *d* density of states with the photoemission data of Seib and Spicer.[16] Sharp structural features, characteristic of pure Ni, persist in the alloy photoemission results up to large Cu concentrations. The CPA is able to account for this.

At the outset, it will be necessary to summarize a few of the CPA results, using notation consistent with VKE. The one-electron Hamiltonian will be assumed to take the form

$$H=W+D=W+\sum_n D_n, \tag{1.1}$$

where W is periodic and D consists of a sum of random contributions, each associated with a single site. The one-electron properties of the alloy are given by an ensemble average over all possible arrangements of the atoms in the lattice, of the Green's function,

$$\langle G(z)\rangle=\langle(z-D-W)^{-1}\rangle\equiv(z-W-\Sigma)^{-1}. \tag{1.2}$$

If the T matrix for a given configuration of the alloy is defined by

$$G=\langle G\rangle+\langle G\rangle T\langle G\rangle, \tag{1.3}$$

an obvious functional equation for the unknown operator Σ is generated:

$$\langle T[\Sigma]\rangle=0. \tag{1.4}$$

Equation (1.4) is a self-consistency condition on the choice of Σ.

Decomposing

$$D-\Sigma=\sum_n (D_n-\Sigma_n)\equiv\sum_n V_n, \tag{1.5}$$

[8] E. A. Owens and L. Pickup, Z. Krist. **88**, 116 (1934).
[9] B. Mozer, D. T. Keating, and S. C. Moss, Phys. Rev. **175**, 868 (1968).
[10] T. J. Hicks, B. Rainford, J. S. Kouvel, G. G. Low, and J. B. Comly, Phys. Rev. Letters **22**, 531 (1969).
[11] J. G. Hanus, MIT Solid State and Molecular Theory Group Quarterly Progress Report No. 44, p. 29, 1961 (unpublished); E. Zornberg, Phys. Rev. B **1**, 244 (1970).
[12] B. Segall, Phys. Rev. **125**, 109 (1962); G. A. Burdick, *ibid.* **129**, 138 (1963).
[13] N. F. Mott and H. Jones, *Theory of the Properties of Metals and Alloys* (Dover Publications, Inc., New York, 1958).
[14] L. Hodges, H. Ehrenreich, and N. D. Lang, Phys. Rev. **152**, 505 (1966).
[15] F. Mueller, Phys. Rev. **148**, 636 (1966).
[16] D. H. Seib and W. E. Spicer, Phys. Rev. Letters **20**, 1441 (1968); D. H. Seib (private communication).

we may define a local scattering operator

$$T_n = V_n(1-\langle G\rangle V_n)^{-1}, \tag{1.6}$$

which describes the effect of replacing the effective medium, characterized by Σ, by the true atom at the given site n. The CPA replaces the general self-consistency condition (1.4) by its single-site approximation[1]:

$$\langle T_n[\Sigma]\rangle = 0, \tag{1.7}$$

which states that the average effect of substituting a true atom at a given site in the effective crystal is zero.

II. SINGLE BAND OF GENERAL SHAPE

In this section we discuss, within the CPA, the effects of alloying upon a nondegenerate band of general shape, described by a simple model Hamiltonian. The more complicated case of degenerate bands is examined in later sections. As in VKE,[4] the single-band model Hamiltonian, when expressed in a Wannier basis in a tight-binding form

$$H = \sum_n |n\rangle\epsilon_n\langle n| + \sum_{n\neq m} |n\rangle t_{nm}\langle m|, \tag{2.1}$$

can usefully be separated into [cf. (1.1)]

$$H \equiv D + W, \tag{2.2}$$

where the off-diagonal elements of W are assumed to have the periodicity of the lattice. However, the diagonal elements ϵ_n of D are random functions of the site index. For a binary substitutional alloy A_xB_y they take on the values ϵ^A and ϵ^B, where

$$\epsilon^A = \tfrac{1}{2}\delta w, \quad \epsilon^B = -\tfrac{1}{2}\delta w, \quad \delta = w^{-1}(\epsilon^A - \epsilon^B), \tag{2.3}$$

and w is a scaling parameter equal to half the bandwidth and x, $y=1-x$ are, respectively, the concentrations of A and B atoms. We shall set $w=1$ in all calculations.

A periodic crystal limit is reached by setting $\delta=0$. Quantities obtained in this limit will be denoted by the superscript (0). For example, the Green's function and the density of states are given, respectively, by

$$G^{(0)}(z) = (z-W)^{-1} \tag{2.4}$$

and

$$\begin{aligned}\rho^{(0)} &= -\pi^{-1}\,\mathrm{Im}(1/N)\,\mathrm{Tr}[G^{(0)}(E+i0)] \\ &= -\pi^{-1}\,\mathrm{Im}\langle 0|G^{(0)}(E+i0)|0\rangle \\ &\equiv -\pi^{-1}\,\mathrm{Im}F^{(0)}(E+i0).\end{aligned} \tag{2.5}$$

More generally, we define

$$F(z) = \langle 0|\langle G(z)\rangle|0\rangle. \tag{2.6}$$

When δ is nonzero, the random terms in D will give rise to a scattering correction to $\Sigma(z)$ which, in the single-site approximation, is site-diagonal and will give a k-independent contribution to matrix elements of Σ between Bloch states. Thus, Σ will take the form

$$\Sigma_{\mathrm{op}} = \Sigma(z)\times\mathbf{1}. \tag{2.7}$$

Equation (2.7) implies a very simple form for the averaged Green's function:

$$\langle G\rangle = [z-W-\Sigma(z)]^{-1} = G^{(0)}(z-\Sigma(z)), \tag{2.8}$$

$$F(z) = F^{(0)}(z-\Sigma(z)). \tag{2.9}$$

The random potential $D-\Sigma$ may be decomposed as in (1.5), to yield

$$V_n = |n\rangle(\epsilon_n-\Sigma(z))\langle n|. \tag{2.10}$$

Because V_n is site diagonal, the local t matrices defined by (1.6) have the simple Koster-Slater[17] form

$$T_n = |n\rangle(\epsilon_n-\Sigma(z))\{1-[\epsilon_n-\Sigma(z)]F^{(0)}(z)\}^{-1}\langle n|. \tag{2.11}$$

The single-site self-consistency condition (1.7), when applied to (2.11), leads to the equation for $\Sigma(z)$.

$$\Sigma = \epsilon + [\Sigma-\epsilon^A]F(z)[\Sigma-\epsilon^B], \tag{2.12}$$

first derived by Soven.[1] In (2.12), we have denoted the average of the diagonal elements by ϵ:

$$\epsilon = \langle\langle 0|D|0\rangle\rangle = x\epsilon^A + y\epsilon^B. \tag{2.13}$$

Equation (2.12) for $\Sigma(z)$ requires only knowledge of $F^{(0)}(z)$, not complete specification of W. Because $F^{(0)}(z)$ is analytic except for a branch cut along the real axis, the Kramers-Kronig relationship,

$$F^{(0)}(z) = \int_{-\infty}^{+\infty} \frac{dE}{z-E}\rho^{(0)}(E), \tag{2.14}$$

completely specifies $F^{(0)}$ in terms of the density of states in the unperturbed crystal.

To construct a form of $F^{(0)}(z)$ that is useful for calculation, we shall approximate the density-of-states function $\rho^{(0)}(E)$ to the accuracy desired by a straight-line interpolation connecting the points $\rho^{(0)}(E_i)$. The edges of the band are taken to be at E_0 and E_n. The resulting $F^{(0)}$ takes the form

$$F^{(0)}(z) = \sum_{i=0}^{n} a_i(z-E_i)\ln(z-E_i). \tag{2.15}$$

The coefficients a_i may be found by evaluating the integral in (2.14), or by using (2.5) in each of the intervals between E_i's. The second procedure is used in Appendix A to show that the a_i are the differences in slopes between the segments of the interpolated density of states to both sides of the points E_i.

Form (2.15) for $F^{(0)}$ will be used in the numerical calculations for NiCu reported below. It has also been applied successfully by Liebermann *et al.*[18] to a tight-

[17] G. F. Koster and J. C. Slater, Phys. Rev. **96**, 1208 (1954).
[18] K. Liebermann, B. Velický, and H. Ehrenreich, Bull. Am. Phys. Soc. **14**, 320 (1969).

binding band with only nearest-neighbor overlap in a simple cubic lattice. Equation (2.15) is the simplest form representing $F^{(0)}$ to guarantee that the real part of $F^{(0)}$ remains finite for all real E, thereby facilitating rapid convergence of the Newton-Raphson iteration[19] used to solve the CPA equation.

The following procedure was used to solve (2.12) by iteration for the cases treated in this paper. The equation is first solved at a real energy sufficiently far below the band for ϵ to provide a good first approximation to the root Σ, then solved again at energies increasing into the band. At each step, the value of Σ calculated for the preceding value of E furnishes a starting approximation for the iteration scheme. It is possible to proceed in this manner at least as far as $E=-\epsilon$, at which point the self-energy may, as discussed in Eq. (4.37) of VKE, be singular. Then the process is repeated, starting above the band and working down.

In the remainder of this section we will study in some detail a simple model, referred to as the "steeple" model, to isolate the consequences when sharp structure and over-all asymmetry, such as that encountered in Ni or in Cu, occur in the model density of states. This consists of a sharp peak, one-tenth as wide as the whole band, located at the top of the band, and a low, wide "shoulder" region. The real and imaginary parts of $F^{(0)}(E+i0)$ in this model are shown in Fig. 1. The density of states is proportional to the latter. The former is seen to vary smoothly near the kinks in $\mathrm{Im}(F^{(0)})$, and

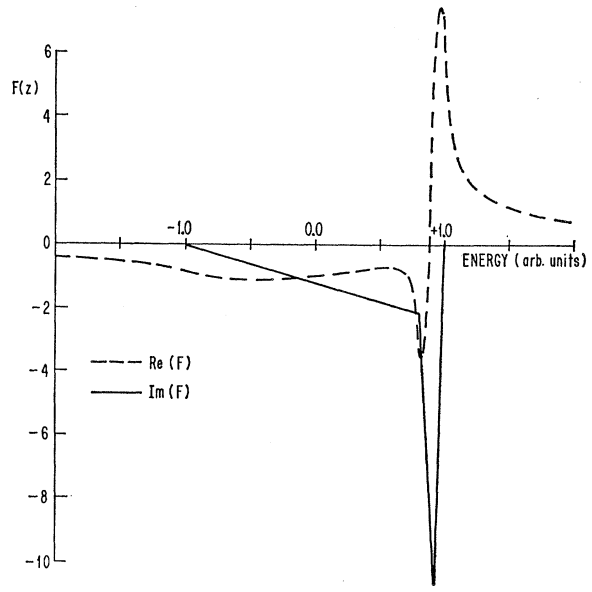

FIG. 1. Real (dashed line) and imaginary (solid line) parts of $F(E+i0)$ for the steeple model density of states, which is proportional to the imaginary part of F.

[19] D. R. Hartree, *Numerical Analysis* (Oxford University Press, New York, 1952), p. 194 ff., or any basic text on numerical analysis.

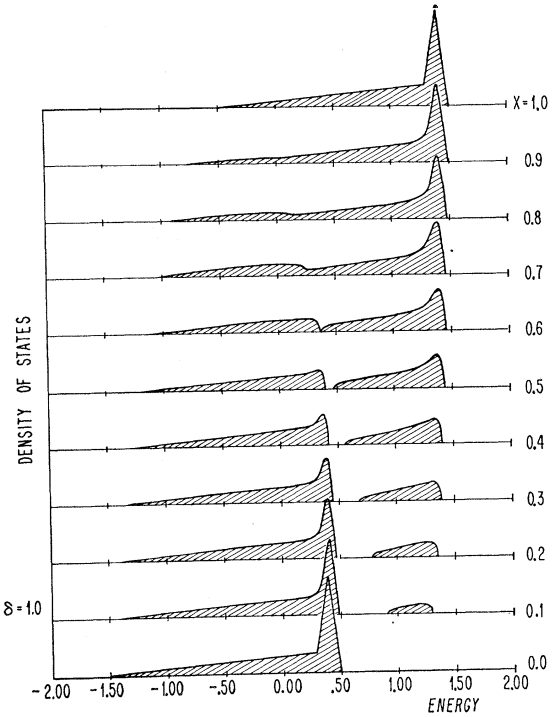

FIG. 2. Density of states calculated in the CPA for the steeple model, with $\delta=1.0$, and x varied in steps of 0.1 from 0.0 to 1.0. Lack of $x\rightarrow(1-x)$ symmetry resulting from the asymmetry of the band is evident.

avoids the spurious singularities characteristic of standard histogram interpolations.

In the low-concentration regime, the Koster-Slater[17] criterion for the occurrence of an impurity state,

$$(1-\delta F^{(0)}(E_0+i0))\,|_{E_0=\text{band edge}}=0\,, \qquad (2.16)$$

can be seen by inspection of Fig. 1 to give different results at the top and bottom of the band. It is possible to split off a state above the peak when $\delta\approx 0.2$, but δ must be almost -1.4 to pull a state away from the shoulder region. To explain this asymmetry, we note that while scattering comparable in strength to the 0.2 unit width of the steeple is sufficient to split off an impurity level at the upper band edge, the extra scattering strength required to make the level appear below the band is necessary in order to translate the impurity state through the shoulder region. This interpretation is substantiated by consideration of models with more extreme asymmetry.[20] It is important here because it indicates how the size of the structural features in the model density of states will influence the physical behavior of the alloy. The same will be seen to be true at finite concentrations, in the CPA.

The concentration dependence of the alloy state density is studied for the steeple model in Fig. 2, where

[20] S. Kirkpatrick, thesis, Harvard University, 1969 (unpublished).

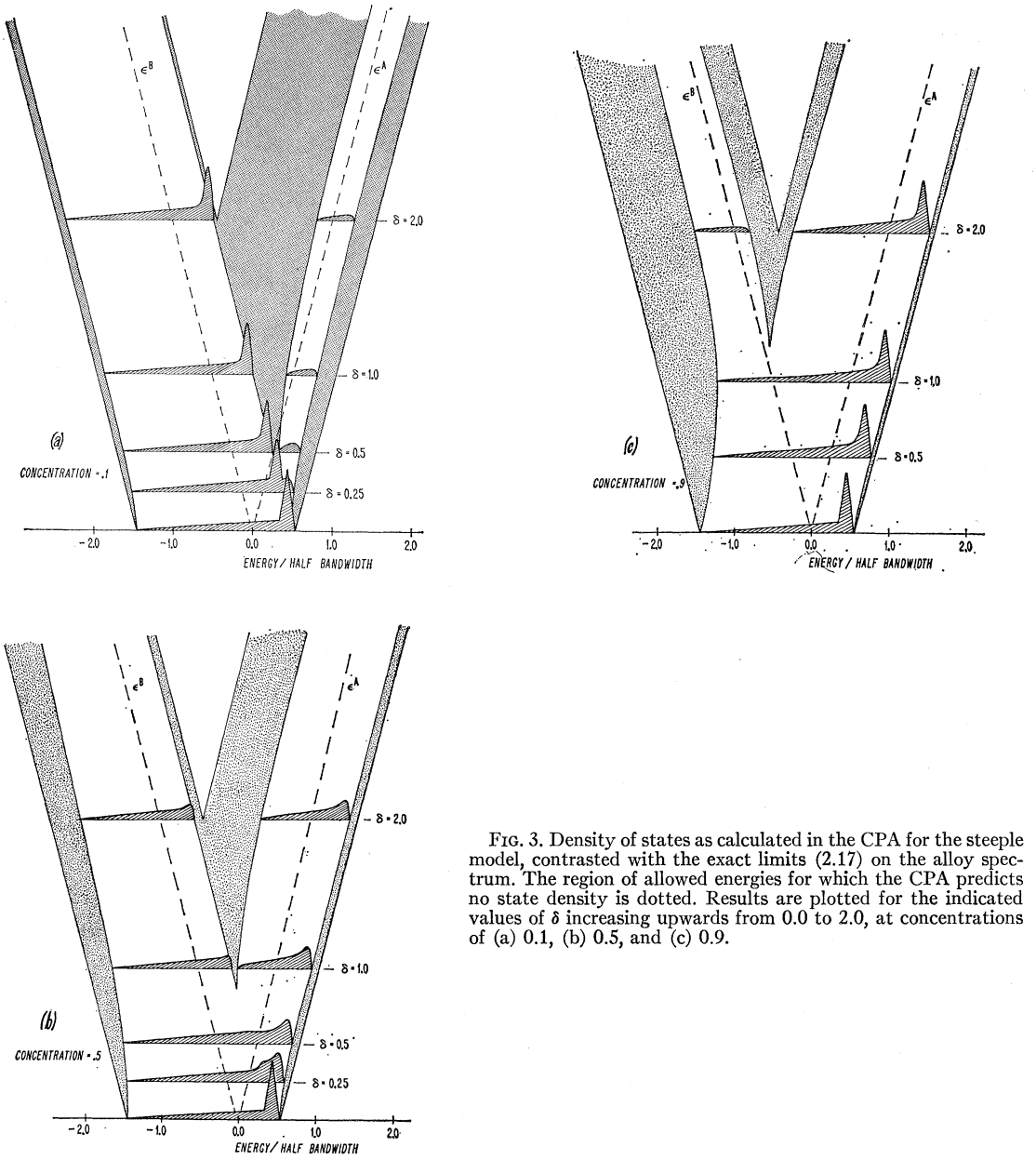

FIG. 3. Density of states as calculated in the CPA for the steeple model, contrasted with the exact limits (2.17) on the alloy spectrum. The region of allowed energies for which the CPA predicts no state density is dotted. Results are plotted for the indicated values of δ increasing upwards from 0.0 to 2.0, at concentrations of (a) 0.1, (b) 0.5, and (c) 0.9.

results for a range of A concentrations $x=0$–1 are shown for $\delta=1$. While this value of δ was sufficient to produce band splitting at all concentrations for the simple model density studied in VKE, such splitting is seen in Fig. 2 only for concentrations less than 0.5. The two main subbands do not shift much with concentration, but remain nearly fixed in energy as the concentration x decreases from 50%. In fact, at all concentrations there appear majority and minority regions of the density of states, one growing as the other declines with concentration. This behavior is characteristic of the "split-band" limit, in which the scattering strength exceeds the bandwidth.[4] Here, however, δ is to be compared to the peak width; it is five times as large.

The asymmetry between effects at the top and at the bottom of the band continues to be apparent in Fig. 2. In the results shown for $x=0.8$ and 0.9, the regions of impurity states seen mixed in the shoulder are much broader than the corresponding split-off bands observed for $x=0.2$ and 0.1. Finally, we note that the split-off majority sub-band, or the region of an unsplit density of states to which the majority components make the dominant contribution, has nearly the full structure and asymmetry of the pure material. By contrast, the asym-

metry of the minority region of the density of states is greatly reduced, and its structure almost nonexistent.

The CPA has been shown[3,4] to extrapolate in a physically reasonable manner into the regimes of moderate concentration and scattering strength. By performing the analysis complementary to that of the preceding figure, holding x fixed and varying δ, we can obtain information about the extent to which the CPA's single-site averaging adequately describes the true density of states. Figures 3(a)–3(c) show the alloy state densities for $x=0.1$ (a), 0.5 (b), and 0.9 (c), each for several values of δ. The results fall within the exact bounds on all possible spectra of the model alloy Hamiltonian which are indicated by the outer boundaries of the V-shaped regions in the three figures. These bounds are defined by a theorem which states that the model Hamiltonian (2.1) can have no eigenstates with energies outside the union of the two intervals,

$$(-\tfrac{1}{2}\delta+E_{\min},\ -\tfrac{1}{2}\delta+E_{\max})(+\tfrac{1}{2}\delta+E_{\min},\ +\tfrac{1}{2}\delta+E_{\max}), \tag{2.17}$$

where $E_{\max}$ and $E_{\min}$ are the edges of the band in the pure crystal. Lifshitz[7] has given intuitive arguments to suggest that every energy within the bounds (2.17) is in fact an eigenvalue of some configuration of (2.1). Because there appears to exist no compact and comprehensive discussion of these theorems in the literature, the necessary proofs are summarized in Appendix B.

The regions of energy allowed by (2.17) for which the CPA predicts no density of states have been dotted in Figs. 3(a)–3(c). These regions may be occupied when approximations transcending the CPA are applied. The resulting states will be associated with "clustering," e.g. local departures from stoichiometry, and will contribute tails or other structure to the state density in the dotted region. Since the number of states in the band, and, as shown in Appendix B, each split sub-band as well, is fixed, the formation of tails will be compensated for by a draining off of states in the CPA band.

For $x=0.1$, illustrated in Fig. 3(a), an impurity band splits off above the peak at $\delta=0.3$, and both majority and minority sub-bands rapidly assume their strong-scattering limiting forms. Once split off, the majority band almost fills its localization region, leaving little room for tailing effects. On the other hand, the tails associated with the impurity sub-band may spread over such a large region of energy that the true density of states could differ greatly from the CPA result. Because in Fig. 3(a) the impurity sub-band splits off at so small a value of δ, the density of states in the vicinity of the upper edge is strongly distorted even at the smallest nonzero values of δ considered. No value of δ treated was small enough for the weak-scattering limit, in which

$$\Sigma(z)\approx\epsilon, \tag{2.18}$$

to be applicable.

The second case, for $x=0.5$, in Fig. 3(b), is also very sensitive to alloying. With increasing δ the principal peak splits. The lower peak overlaps the shoulder region and becomes increasingly broad as it moves toward the bottom of the band. This behavior parallels the continuum broadened impurity levels appearing in the dilute alloy.[21] In the strong-scattering regime, the sharp corners, resembling critical points, are rounded over. The upper band edges of the two split sub-bands, near which most of the density of states is concentrated, fall nearer to the exact spectral limits than do the lower shoulderlike edges. Thus the clustering effects not considered in the CPA should have less effect upon the upper edges than on the lower edges.

As shown in Fig. 3(c), for $x=0.9$, the resonance is too strongly damped to be observable in the shoulder region at small δ. Increasing δ from zero merely causes the band to broaden, until at $\delta\simeq1.4$ the impurity band finally splits off.

As in Fig. 3(a) ,the majority sub-band, once split, nearly fills its localization region, but the sharp structure in this sub-band appears to be somewhat less rounded off at a given value of δ than is the structure in the majority sub-band for the case $x=0.1$. By comparing Fig. 3(c) with Fig. 3(a), the impurity sub-band emerging from the shoulder can be seen to be wider and more symmetric than the sub-band split off above the peak by a δ of the same magnitude.

III. MODEL HAMILTONIAN FOR *Ni*Cu

Construction of a model Hamiltonian to describe *Ni*Cu requires some picture of the crystal potential in the alloy. This is a difficult problem in general, but fortunately less so in the case of *Ni*Cu. The fact that the dimensions of the Wigner-Seitz cell are almost identical in Ni, in Cu, and in their alloys suggests as a starting approximation that we place on Ni and Cu sites in the alloy the atomic Hartree-Fock potentials in the configurations appropriate to the calculation of the respective band structures of the pure metals. The high energy cost associated with departures from charge neutrality in each cell suggest that the neutral configurations will be approximately self-consistent in the alloy. Band structures in agreement with existing experimental data have been obtained for Ni [11] and for Cu [12] in the Hartree-Fock approximation, starting with atomic $3d^n4s$ configurations. It is not surprising that the resulting plane-wave-like bands are nearly identical outside of the region in which hybridization with the d bands takes place. In each case there is roughly one non-d electron per atom in the crystal.

From these comparisons, we expect the s bands in *Ni*Cu to be unaffected by alloying, and concentrate our attention on the alloy's tight-binding-like d bands. Thus the alloy states may be expressed in a basis of a few reciprocal-lattice vectors and five tight-binding d functions, whose construction is discussed in detail below. We shall derive a model Hamiltonian for this basis in

[21] J. Friedel, Suppl. Nuovo Cimento 7, 287 (1968).

the form of the combined interpolation schemes of Refs. 14 and 15. The problem of determining the alloy potential has thereby been reduced to that of specifying a few matrix elements of that potential. Explicit consideration of correlation effects between d electrons will be unnecessary, as we are interested in the properties of the alloys above their Curie temperatures.

Further comparison of the Cu and Ni band structures shows that the Cu d bands lie lower than those of Ni, and are somewhat narrower. Since pure Cu and pure Ni correspond to the endpoints of the alloy series, these differences determine the effects of alloying on the d-d block of the alloy model Hamiltonian. To discuss this block we must first transform it from the customary Bloch tight-binding basis into a basis of atomic orbitals. In this form we write the d-d block of the model Hamiltonain as

$$H_{dd}=\sum_n |\mu n\rangle \epsilon_{\mu n} \langle \mu n| + \sum_{n\neq n',\mu,\mu'} |\mu n\rangle t_{\mu n,\mu' n'} \langle \mu' n'| \,, \quad (3.1)$$

where the $|\mu n\rangle$ represents a d orbital, centered on the nth site. If μ is 1, 2, or 3, the orbital has t_{2g} symmetry about its site; if μ is 4 or 5, the symmetry is e_g. A Ni oribtal is used if the site n is a Ni site, and similarly for Cu.

The shift of the d bands may be accounted for by letting the $\epsilon_{\mu n}$ take values appropriate to pure Cu and pure Ni on Cu and Ni sites, respectively. The narrowing implies some random behavior for the $t_{\mu n,\mu' m}$. However, the effects associated with randomness among the off-diagonal elements cannot be separated in the form of (1.1) into independent contributions from each site, so they are intractable in the present form of the CPA. Therefore, we shall require that the off-diagonal part of the d-d matrix (3.1) be translationally invariant, and set the $t_{\mu n,\mu' m}$ equal to their values for pure Ni, in order to discuss the Ni-rich alloys. It would be possible to give the off-diagonal elements some heuristic concentration dependence without removing the requirement of translational invariance. We have not done this, since experience with the single-band model[4] has shown that a wealth of physical behavior can be obtained from a model with only diagonal alloying effects.

As a final justification for this approximation, we note that direct evaluation of the tight-binding matrix elements of (3.1), using the atomic Hartree-Fock orbitals and potentials for Ni and Cu, shows that the variation in the alloy of any off-diagonal element is small with respect to the difference between diagonal elements since the differences between the two potentials are both quite localized near the center of the atomic cell and contribute little to two-center integrals. Moreover, effects of alloying on the off-diagonal elements of the Hamiltonian (3.1), although they do cause the change in width, cannot alter the basic topology of the d bands. Therefore, we feel that the procedure of treating only the diagonal effects of alloying is a physically reasonable one.

It remains only to determine the size of the splitting δ between Ni and Cu d states. This is the same for the two orbital symmetries, since crystal field terms are small in both Cu and Ni, and can be determined by comparing the values of the parameter E_0, which in Hodges's[22] notation takes the place of $\epsilon_{\mu n}$ in the absence of crystal field splitting, in the interpolation Hamiltonians for Ni and Cu. E_0 proves to be 0.06 Ry greater in Ni than in Cu, when referred to the point Γ_1 as origin. We make this choice of origin because, as noted above, the s bands in Ni and in Cu are nearly identical, and are assumed to be unchanged in the alloy.

As a check, we can also estimate the splitting δ by comparing the positions of the $3d$ levels of the neutral atoms in the $3d^n4s$ configurations, using atomic potentials modified to include the increased screening in the solid due to the higher s-electron density in the core region.[23] In these modified potentials, the $3d$ states lie above the $4s$ levels, as the associated bands would in a solid. Comparing in each case the $3d$ energy with the $4s$ energy, which can be shown[23] to fall roughly at the mean energy of a singly occupied s band in the solid, we find again a shift of 0.06 Ry between Ni and Cu $3d$ energies. Our model Hamiltonian's d-d block, as constructed in the localized basis, consists simply of the corresponding d-d Hamiltonian for pure Ni, with all the diagonal elements of Cu sites shifted down by 0.06 Ry.

IV. CPA FOR INTERPOLATION HAMILTONIAN

We shall now study the properties of the full interpolation Hamiltonian for a NiCu alloy, using the d-d block derived in Sec. III, and extending the CPA to treat the d bands in the presence of hybridization and orbital degeneracy. This Hamiltonian, expressed in a basis of tight-binding Bloch functions and orthogonalized plane waves, will be separated into a random part D and a configuration-independent part W:

$$H=W+D=\begin{pmatrix} W_{ss} & W_{sd} \\ W_{ds} & \begin{matrix} W_{EE} & W_{ET} \\ W_{TE} & W_{TT} \end{matrix} \end{pmatrix} + \begin{pmatrix} 0 & 0 \\ 0 & \begin{matrix} D_{EE} & 0 \\ 0 & D_{TT} \end{matrix} \end{pmatrix}. \quad (4.1)$$

The various blocks in (4.1) are labeled by the indices s for the plane-wave-like states, d for the tight-binding d states, and E or T for d states constructed from atomic orbitals of e_g or t_{2g} symmetry, respectively. Although the basis functions used in defining (4.1) are not translationally invariant because of the site-dependent assignment of orbitals, we assume configuration-independent and translationally invariant matrix elements W. We shall set them equal to the appropriate elements of the interpolation Hamiltonian describing pure Ni; thus they are concentration-independent as well. The details of

[22] L. Hodges, thesis, Harvard University, 1966 (unpublished), Appendices.

[23] L. Hodges, R. E. Watson, and H. Ehrenreich, Phys. Rev. Letters 24, 829 (1970).

the interpolation Hamiltonian, and the fitting of its parameters, are contained in Refs. 14 and 22.

It will prove useful to express the elements of the random d-d block D in terms of the matrix elements of some simple projection operators. The basic projectors are P_{nE} and P_{nT}, which select the subspace of e_g or t_{2g} symmetry about the site n, and have the properties

$$P_{nE}P_{mE}=\delta_{nm}P_{nE}, \quad P_{nT}P_{mT}=\delta_{nm}P_{nT}, \quad P_{nE}P_{mT}=0. \tag{4.2}$$

Other projection operators may be constructed from these to select all d states at a given site, or all states of a given symmetry in the crystal:

$$P_n=P_{nE}+P_{nT}, \quad P_E=\sum_n P_{nE}, \quad P_T=\sum_n P_{nT}. \tag{4.3}$$

Useful operators are also obtained by summing only over Ni or Cu sites in the alloy:

$$P^{\mathrm{Ni}}=\sum_{(\mathrm{Ni})} P_n, \quad P^{\mathrm{Cu}}=\sum_{(\mathrm{Cu})} P_n, \qquad P_E{}^{\mathrm{Ni}}=P_EP^{\mathrm{Ni}}, \text{ etc.} \tag{4.4}$$

All of these subdivide the subspace selected by P, the operator projecting onto all d states:

$$P=P_E+P_T=P^{\mathrm{Ni}}+P^{\mathrm{Cu}}=\sum_n P_n. \tag{4.5}$$

The operator D, given by (3.1), when expressed in terms of the operators of (4.2),

$$\begin{aligned} D&=\Sigma_nD_n=\Sigma_n(\epsilon_{nE}P_{nE}+\epsilon_{nT}P_{nT}) \\ &=\epsilon_E{}^{\mathrm{Ni}}P_E{}^{\mathrm{Ni}}+\epsilon_T{}^{\mathrm{Ni}}P_T{}^{\mathrm{Ni}}+\epsilon_E{}^{\mathrm{Cu}}P_E{}^{\mathrm{Cu}}+\epsilon_T{}^{\mathrm{Cu}}P_T{}^{\mathrm{Cu}}, \end{aligned} \tag{4.6}$$

is seen to be a sum of single-site scattering contributions. Its effects will be treated by using the CPA to define an appropriate effective self-energy such that, in the single-site approximation,

$$\langle G\rangle=\langle(z-W-D)^{-1}\rangle=(z-W-\Sigma)^{-1}. \tag{4.7}$$

Although the configuration-dependent basis set used in deriving (4.1) precludes associating an operator in real space with the averaged matrix $\langle G\rangle$, we may use (4.7) to obtain physical quantities, such as the average density of states per atom:

$$\rho(E)=-(\pi N)^{-1}\,\mathrm{Im}\,\mathrm{Tr}\langle G(E+i0)\rangle. \tag{4.8}$$

Equation (4.8) may be decomposed, using the projection operators, into the contributions from different types of states:

$$\rho=\rho_s+\rho_d=\rho_s+\rho_E+\rho_T, \tag{4.9}$$

where

$$\rho_s=-(\pi N)^{-1}\,\mathrm{Im}(\mathrm{Tr}(1-P)\langle G\rangle), \tag{4.10a}$$

$$\rho_E=-(\pi N)^{-1}\,\mathrm{Im}(\mathrm{Tr}P_E\langle G\rangle), \tag{4.10b}$$

and

$$\rho_T=-(\pi N)^{-1}\,\mathrm{Im}(\mathrm{Tr}P_T\langle G\rangle). \tag{4.10c}$$

Since ρ_s is small, we shall be primarily concerned with the d-state densities ρ_E and ρ_T. When the exact Σ, or any reasonable approximation to it, is used in (4.7), ρ_E and ρ_T satisfy simple sum rules:

$$\int dE\,\rho_E(E)=2, \quad \int dE\,\rho_T(E)=3. \tag{4.11}$$

Because D, as noted in (4.6), is site-diagonal, both the scattering matrix T_n and the self-energy Σ, in the single-site approximation, will be site-diagonal:

$$\Sigma=\sum_n P_n\Sigma_nP_n. \tag{4.12}$$

T_n is obtained by a simple generalization of (2.11) to the subspace of the five d orbitals. Application of the self-consistency condition (1.7) yields the CPA equation[1]

$$\Sigma_n=\langle D_n\rangle-(D_n{}^{\mathrm{Cu}}-\Sigma_n)P_n\langle G\rangle P_n(D_n{}^{\mathrm{Ni}}-\Sigma_n), \tag{4.13}$$

analogous to (2.12).

Because Σ_n and $P_n\langle G\rangle P_n$ are properties of the averaged crystal, they must have the fcc point symmetry. Therefore, we have

$$\Sigma_n=\Sigma_EP_{nE}+\Sigma_TP_{nT}, \tag{4.14}$$

and

$$P_n\langle G\rangle P_n=F_EP_{nE}+F_TP_{nT}. \tag{4.15}$$

Here $\Sigma_{E,T}$ and $F_{E,T}$ are site-independent scalar quantities. Substituting (4.15) and (4.14) into (4.13) yields two scalar equations for Σ_E and Σ_T:

$$\Sigma_E=\langle\epsilon_E\rangle-(\epsilon_E{}^{\mathrm{Cu}}-\Sigma_E)F_E(\epsilon_E{}^{\mathrm{Ni}}-\Sigma_E), \tag{4.16a}$$

$$\Sigma_T=\langle\epsilon_T\rangle-(\epsilon_T{}^{\mathrm{Cu}}-\Sigma_T)F_T(\epsilon_T{}^{\mathrm{Ni}}-\Sigma_T). \tag{4.16b}$$

Although each of the equations (4.16) has exactly the form of the single-band case (2.12), they are coupled through the implicit dependence of F_E and F_T on both Σ_E and Σ_T. There is no simple relation of the form (2.9) to represent, for example, $F_E(z)$ in terms only of Σ_E and the unperturbed Green's function.

By an explicit calculation of F_E, we shall now describe its dependence on Σ_E and ϵ_T, and develop an approximate method of decoupling the Eqs. (4.16). The technique to be used is the partitioning method of Löwdin.[24] Given an operator A and a projector Π, the operator (Π/A) is defined by

$$\Pi A\Pi(\Pi/A)=(\Pi/A)\Pi A\Pi=\Pi A\Pi. \tag{4.17}$$

It can be shown that

$$\Pi A^{-1}\Pi=\frac{\Pi}{A-\Pi A[(1-\Pi)/A]A\Pi}. \tag{4.18}$$

Using this procedure, we may evaluate

$$\begin{aligned} F_E&=(2N)^{-1}\mathrm{Tr}P_E\langle G\rangle P_E \\ &=(2N)^{-1}\,\mathrm{Tr}P_E(z-W-\Sigma_EP_E-\Sigma_TP_T)^{-1}P_E \end{aligned} \tag{4.19}$$

[24] For example, P. O. Löwdin, J. Appl. Phys. **33**, Suppl. 1, 251 (1952).

by inspection. However, (4.19) is first rewritten, using

$$P_E\langle G\rangle P_E=P_E(P\langle G\rangle P)P_E, \tag{4.20}$$

and the partitioning proceeds in two stages, the first, using (4.18) inside the parentheses of (4.20), to separate the s from the d states, the second to obtain the e_g contribution. The result is

$$F_E(z)=(2N)^{-1}\,\mathrm{Tr}(P_E/L_E), \tag{4.21a}$$

where

$$L_E=z-W_{EE}-\Sigma_E-Q_{EE}-[W_{ET}+P_EQ] \times[P_T/(z-\Sigma_T-W_{TT}-Q_{TT})][W_{TE}+Q_{TE}]. \tag{4.21b}$$

The quantity $Q(z)$, which contains all the effects of hybridization, is defined by

$$Q(z)=W_{ds}\frac{1-P}{z-W_{ss}}W_{sd}. \tag{4.22}$$

In (4.21), Σ_T is seen to affect F_E only through the final term in the denominator, which describes coupling, both direct and indirect via hybridization, between the e_g and the t_{2g} states.

If the energies entering (4.21) are redefined slightly by introducing

$$\Delta_E=\Sigma_E-\epsilon_E{}^{\mathrm{Ni}},\quad \Delta_T-\Sigma_T-\epsilon_T{}^{\mathrm{Ni}}, \tag{4.23}$$

and

$$z'=z-\Delta_E, \tag{4.24}$$

the denominator of (4.11) may be rewritten as

$$z'-\epsilon_E{}^{\mathrm{Ni}}-W_{EE}-Q_{EE}(z'+\Delta_E)-(W_{ET}+P_EQ)[P_T/ (z'+\Delta_E-\Delta_T-\epsilon_T{}^{\mathrm{Ni}}-W_{TT}-Q_{TT})](W_{TE}+QP_E). \tag{4.25}$$

It will now be clear under what conditions a relation of the form (2.9) is valid for (4.25). If $\Delta_E\approx0$, the hybridization term becomes approximately $Q(z')$; if in addition $\Delta_E-\Delta_T\approx0$, the terms describing e_g-t_{2g} mixing depend solely on z'. These criteria are guaranteed, both for this case and for the analogous treatment of F_T, by the conditions

$$\Delta_E\approx0,\quad \Delta_T\approx0. \tag{4.26}$$

If (4.26) holds, we may neglect Δ_E and Δ_T in (4.25), and obtain

$$F_E(z)\approx F_E{}^{\mathrm{Ni}}(z')=F_E{}^{\mathrm{Ni}}(z-\Sigma_E+\epsilon_E{}^{\mathrm{Ni}}), \tag{4.27}$$

and, in like fashion,

$$F_T(z)=F_T{}^{\mathrm{Ni}}(z-\Sigma_T+\epsilon_T{}^{\mathrm{Ni}}). \tag{4.28}$$

In (4.27), $F_E{}^{\mathrm{Ni}}$ is taken to be (4.19) with Σ given by its value for pure Ni, i.e., $\Sigma_E=\epsilon_E{}^{\mathrm{Ni}}$. The definition of $F_T{}^{\mathrm{Ni}}$ in (4.28) is analogous. Now the techniques developed for a single band of general shape in Sec. II may be applied independently to F_E and to F_T. The integral representation,

$$F_E{}^{\mathrm{Ni}}(z)=\frac{1}{2}\int d\eta\frac{\rho_E{}^{\mathrm{Ni}}(\eta)}{z-\eta}, \tag{4.29}$$

implies that the only input information needed for the calculation is the e_g and t_{2g} components of the Ni density of states, and the value obtained in Sec. III for δ.

The conditions (4.26) of course limit the validity of the results obtained in this simple way, but the limitations are not severe. The model Hamiltonian was constructed to describe the region of low Cu concentration, in which Δ_E and Δ_T are expected to be small. The approximation (4.26) appears in (4.25) in two places. The hybridization term Q is a slowly varying function of the energy,[14] and the changes in argument are permissible. The neglect of Δ_E and Δ_T in the denominator of (4.25) may be more important near the band edges.[4] However, a quantitative check is provided by a comparison of the upper edges of the e_g and t_{2g} bands. Without the approximation (4.26), Eqs. (4.16) predict that the two edges coincide. Use of (4.26) leads to a difference in energy between the approximate edges, which, however, is small. The practical benefits of the approximation, which avoids rediagonalization of (4.1) for all values of Σ_E and Σ_T, outweigh these limitations.

With the self-energies calculated from the CPA equations (4.16), we can obtain the components of the alloy density of states by combining (4.10) and (4.15):

$$\begin{aligned}\rho_E(E)&=-(2/\pi)\,\mathrm{Im}F_E(E+i0),\\ \rho_T(E)&=-(3/\pi)\,\mathrm{Im}F_T(E+i0).\end{aligned} \tag{4.30}$$

Even the partial densities of states $\rho_{E,T}{}^{\mathrm{Ni}}$ and $\rho_{E,T}{}^{\mathrm{Cu}}$ coming from Ni and Cu sites, respectively, in the alloy, may be expressed in terms of $\Sigma_{E,T}$ and $F_{E,T}$. For example, $\rho_T{}^{\mathrm{Ni}}$, defined by

$$\rho_T{}^{\mathrm{Ni}}(E)=-\pi^{-1}\,\mathrm{Im}\,\mathrm{Tr}\langle P_T{}^{\mathrm{Ni}}G(E+i0)\rangle, \tag{4.31}$$

may be evaluated by using the expression

$$P_T{}^{\mathrm{Ni}}=\frac{D_{TT}-\epsilon_T{}^{\mathrm{Cu}}}{\epsilon_T{}^{\mathrm{Ni}}-\epsilon_T{}^{\mathrm{Cu}}}P_T \tag{4.32}$$

for $P_T{}^{\mathrm{Ni}}$. Because the projection operator (4.32) is configuration-dependent, the average in (4.31) must be taken over both the Green's function and the projector. The result may be expressed in terms of G in several steps; making use of the form (4.1) of D, we have

$$\begin{aligned}\langle P_T(D_{TT}-\epsilon_T{}^{\mathrm{Cu}})G\rangle&=\langle P_T(H-W-\epsilon_T{}^{\mathrm{Cu}})(z-H)^{-1}\rangle\\ &=P_T(z-W-\epsilon_T{}^{\mathrm{Cu}})(z-W-\Sigma)^{-1}-P_T\\ &=P_T(\Sigma_T-\epsilon_T{}^{\mathrm{Cu}})\langle G\rangle,\end{aligned} \tag{4.33}$$

so that, finally,

$$\rho_T{}^{\mathrm{Ni}}(E)=-(\pi N)^{-1}(\epsilon_T{}^{\mathrm{Ni}}-\epsilon_T{}^{\mathrm{Cu}})^{-1} \times\mathrm{Im}\,\mathrm{Tr}[P_T(\Sigma_T-\epsilon_T{}^{\mathrm{Cu}})\langle G\rangle]. \tag{4.34}$$

This expression, which is exact for the model Hamiltonian (4.1), reduces in the single-site approximation to

$$\rho_T^{\mathrm{Ni}}(E) = -3(\pi N)^{-1}(\epsilon_T^{\mathrm{Ni}} - \epsilon_T^{\mathrm{Cu}})^{-1} \times \mathrm{Im}[(\Sigma_T - \epsilon_T^{\mathrm{Cu}})F_T(E+i0)], \quad (4.35)$$

using (4.14) and (4.15). A quantity similar to (4.34), but valid only within the single-site approximation, was derived in VKE. There the local state density was evaluated at a site containing a Ni atom and surrounded by the effective medium characterized by Σ, then multiplied by the probability that the site contained a Ni atom, yielding

$$\rho_T^{\mathrm{Ni}}(E) = -(N)^{-1}(1-x)\,\mathrm{Im}\{F_T(E+i0)/[1-(\epsilon_T^{\mathrm{Ni}} - \Sigma_T)F_T(E+i0)]\}. \quad (4.36)$$

This was interpreted as the partial density of states per Ni site in the averaged crystal. Using (4.16b) to relate Σ_T and F_T, one can show that (4.35) and (4.36) are equivalent in the CPA. Both definitions (4.35) and (4.36) may be used in other single-site approximations, but they yield different results. While the more general expression (4.35) always satisfies the natural condition

$$\rho_T(E) = \rho_T^{\mathrm{Ni}}(E) + \rho_T^{\mathrm{Cu}}(E), \quad (4.37)$$

definition (4.36) satisfies (4.37) only in the CPA. These results generalize the discussion of the local densities given in VKE.

V. DENSITY OF STATES IN *Ni*Cu ALLOYS

The calculation of the density of states in the *Ni*Cu alloys has now been reduced to a form in which the only input information needed is ρ_T^{Ni}, ρ_E^{Ni}, δ, and x. These determine Σ_T and Σ_E by Eqs. (4.16) and (4.29), and the total and partial densities (4.8), (4.30), and (4.31), as well. The e_g and t_{2g} components of the density of states in Ni can be determined easily in the interpolation scheme, and are shown in Fig. 7 of Ref. 25. The t_{2g} density has two characteristic peaks, while the other is relatively structureless. The work of Ref. 14 showed that the position of the lower peak in the density of states is quite sensitive to hybridization, so the explicit treatment of hybridization of the alloy d bands, as carried out in Sec. IV, is essential for an accurate treatment.

The results of the CPA calculations, using as input 52-point interpolations of the form (2.15) of the t_{2g} and e_g Ni partial densities, are contained in Figs. 4–7. Figure 4 shows the t_{2g} densities for Cu concentrations of 0, 10, 20, 30, 40, 50, and 60%. The strong peaks characteristic of pure Ni and Cu persist in all cases studied, but the effects of alloying are nonetheless strong. At low concentrations, the peaks lose intensity rapidly and broaden slightly, while the many wiggles due to fine features of the density of states are quickly damped out. This process tapers off at a concentration of about 30%, after which the shape of the band changes little. The peaks continue to lose height slowly, and the second peak gains in strength relative to the first. The upper edge of the t_{2g}-state density function shifts very little as a function of concentration.

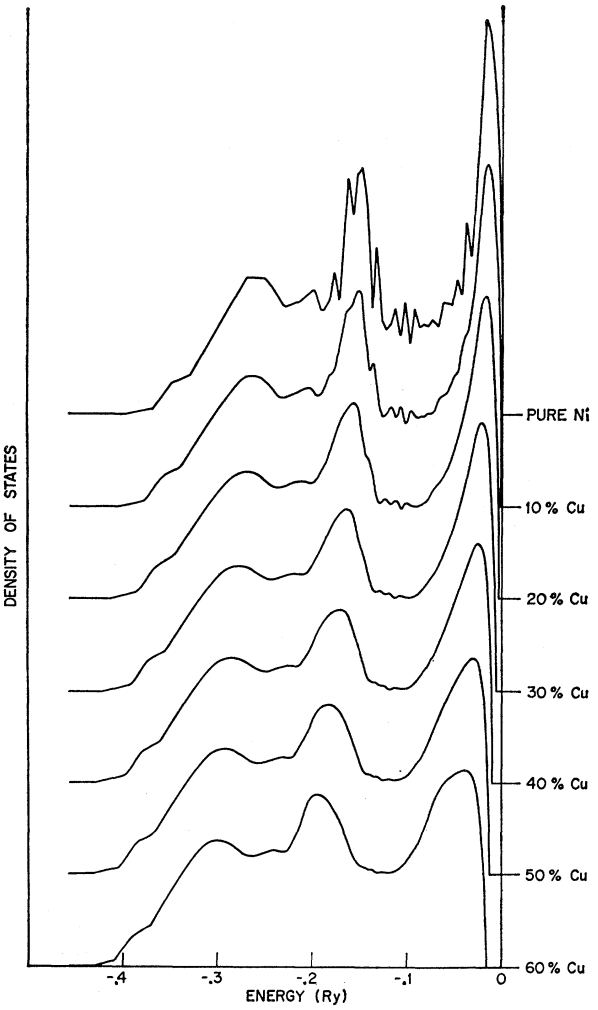

FIG. 4. t_{2g} density of states in *Ni*Cu, calculated in the CPA for the model Hamiltonian (4.1), based upon that of Ni. In this, and the results shown in Figs. 5–7, the splitting between d levels in Ni and Cu is taken to be 0.06 Ry. The concentration, indicated at the right, is increased in steps of 0.1 from pure Ni to 60% Cu. The origins of the curves have been displaced for sake of clarity.

This behavior of the t_{2g} density should be compared with that predicted by the virtual crystal model, which takes the limit (2.18) of weak scattering. The latter predicts that the band will shift uniformly, with no change in structure. Clearly, this does not occur in Fig. 4. Also the shift of the upper edge of 0.03 Ry predicted for the case $x=0.5$ is three times the shift calculated in the CPA. Even if scattering corrections to the virtual crystal limit (see VKE, Eq. 4.20) are included, the resulting changes in structure affect all parts of the band equally. This cannot explain the different behavior noted in Fig.

[25] N. D. Lang and H. Ehrenreich, Phys. Rev. **168**, 605 (1968).

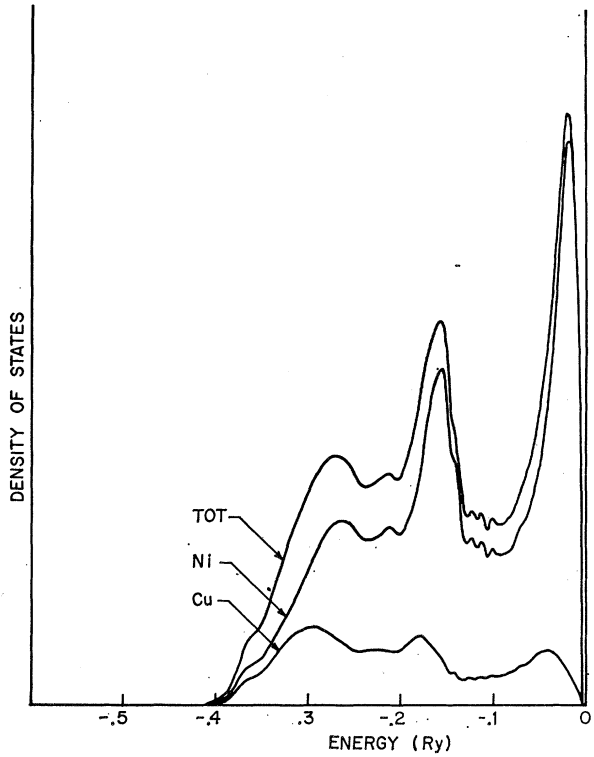

FIG. 5. The average t_{2g} state density, calculated in the CPA for the case 80% Ni, 20% Cu, is separated into its contributions from Ni and from Cu sites in the alloy. These sum to give the total t_{2g} density, denoted "TOT".

4 in the top and bottom of the band, where the bottom half broadens while the separation of the two peaks at the top remains constant. A similar effect was noted in connection with the steeple model in Sec. II, whenever δ exceeded the characteristic size of the steeple.

Because the scattering strength chosen was already strong with respect to the widths of the t_{2g} peaks, the results were not terribly sensitive to the precise value of δ used. The same calculations were performed with δ increased by a factor of 2, with results at low concentrations almost identical to those shown in Fig. 4. At higher concentrations the stronger scattering caused the density of states to be more strongly smeared out than were the corresponding examples for $\delta=0.06$ Ry. Similar conclusions hold true for the sensitivity to δ of the other calculated quantities presented in this section.

Several more detailed features of the calculations are shown in Fig. 5, for the case of 20% Cu. The curves represent the contributions to the average t_{2g} density of states from Ni and from Cu sites, ρ_T^{Ni} and ρ_T^{Cu}, as defined by (4.36), and their sum which, by (4.37), is the net t_{2g} state density in the alloy. To a remarkable extent, the Ni states dominate the top peak, while the Cu states are shifted to lower energies. Although the density of states on the Ni sites closely resembles the pure Ni state density, the density of states on the Cu sites bears little resemblance to that of pure Cu or Ni. Because the Ni partial density is much greater than the Cu component near the top of the d bands, it is clear that in the Ni-rich alloys, for which the Fermi level lies in this region, d holes will be found primarily on the Ni sites. Thus, our conjecture that the Ni and Cu sites would retain the $3d^n4s$ configurations in the alloy is substantiated. This "minimum-polarity" hypothesis, supplemented by some exact results concerning moments from Ref. 4, forms the basis of the simple calculations of the magnetic properties of *Ni*Cu reported in Refs. 25 and 26. This work assumed that the Cu sites did not contribute to the density of states at the Fermi level, and postulated a concentration dependence for the peak at the top of the d band which is roughly similar to that calculated here.

The complete set of calculations for the Ni-rich alloys is summarized in Fig. 6. For the six cases studied, from 10–60% Cu, we plot the t_{2g} and e_g densities of states and their sum, the total state density, ρ_d. The peaks in the total d density of Fig. 6 are almost entirely due to ρ_T. Because ρ_E^{Ni} has little structure, we must compare δ with the over-all bandwidth to determine if the weak-scattering limit applies. Since δ is much less than the bandwidth, virtual-crystal-like behavior is indeed seen in the e_g states in Fig. 6, and their upper edge shifts down more rapidly with concentration than does the top of corresponding t_{2g} state density, where the scattering has been seen to be effectively stronger. As mentioned in Sec. IV, the difference in behavior of the edges is an artifact of our approximate decoupling of the equations governing the states of the two symmetries. Since the inconsistency is not too great, it has simply been ignored in computing ρ_T.

Finally, in Fig. 7, we compare the calculated total densities with the photoemission data of the Stanford group.[16] There are difficulties in the interpretation of

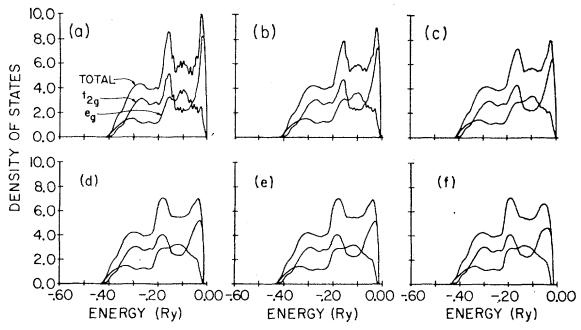

FIG. 6. Total density of d states in *Ni*Cu, calculated in the CPA by adding the t_{2g} and e_g components, properly weighted to account for orbital degeneracy. Results are plotted for concentrations of (a) 0.1 Cu, (b) 0.2, (c) 0.3, (d) 0.4, (e) 0.5, and (f) 0.6. The t_{2g} curves in this figure are also plotted in Fig. 4. The e_g state densities were obtained by the same procedure as were the t_{2g} densities, using the same value for the atomic splitting.

[26] S. Kirkpatrick, B. Velický, H. Ehrenreich, and N. D. Lang, J. Appl. Phys. **40**, 1283 (1969).

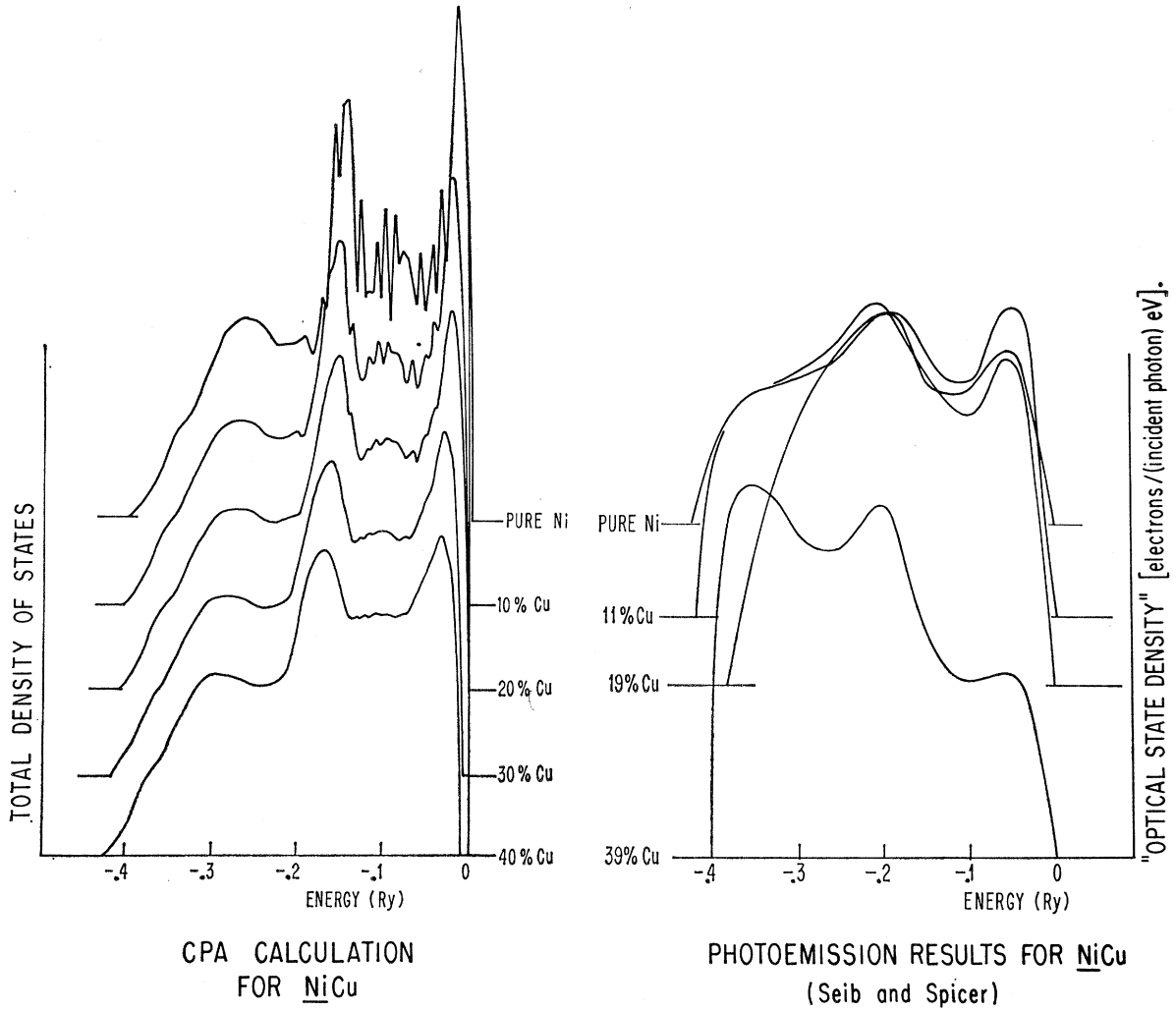

FIG. 7. The CPA total *d* state densities, shown in Fig. 6, are compared with the "optical state density" of Seib and Spicer (Ref. 16). The persistence of the two peaks in the experimental data is especially to be noted.

these data, since they involve a joint density of states to whose structure, however, the final states probably do not contribute significantly. Furthermore, electrons initially from the upper parts of the band which have lost energy by scattering before leaving the sample may be confused with those originally from the bottom of the band. However, at the top of the band, where the experiment is best, the photoemission data of Fig. 7 show that the peaked structure is present at all concentrations, that the separation in energy between the two peaks is constant, and that the second peak grows relative to the first at large Cu concentrations. All three features are also found in the CPA calculations. We have already pointed out the persistence of the two peaks in the CPA results. The increase in strength of the lower part of the band, especially the second peak at larger Cu concentrations is due to the broad, rather shapeless Cu contribution to the density of states, which is largest at lower energies. However, the constant separation between the two peaks in the calculated results is probably a trivial consequence of our assumption that the off-diagonal elements of the Hamiltonian are unaffected by alloying. This point will have to be checked by a calculation with a model Hamiltonian more sophisticated than (4.1).

The CPA calculations on *Ni*Cu reported here have several important consequences. As just noted, the features of the photoemission data for this system can be explained by use of the present model. Further, the assumptions on which the model Hamiltonian was constructed were found to be roughly self-consistent. They therefore support our previously reported studies of the magnetic properties.[20,26]

Finally, the study of the effects of alloying on sharp structure in the density of states shows why the weak-scattering models, such as the rigid-band model, often

adduced to explain the behavior of transition metal alloys, often fail. Our model, by requiring as input only the density of states in pure Ni avoids speculating on the fine details of the Hamiltonian in the crystal. The good agreement between the calculations and various experiments shows the CPA to be a potentially useful tool for quantitative studies of these alloys.

APPENDIX A: FITTING AN ARBITRARY $F^{(0)}$

The density-of-states function $\rho^{(0)}(E)$ will be approximated by straight-line interpolation between the points $\rho^{(0)}(E_i)$ which we denote ρ_i. E_0 and E_n denote the band edges. The interpolated density of states is given, for F in the interval between E_{i-1} and E_i, by

$$\rho(E)=\rho_i+b_i(E-E_i), \tag{A1}$$

where the slope b_i is

$$b_i=(\rho_i-\rho_{i-1})/(E_i-E_{i-1}). \tag{A2}$$

At the edges, ρ_0 and $\rho_n=0$, and we specify that b_0 and $b_{n+1}=0$.

The form assumed for $F^{(0)}(z)$ in Sec. II,

$$F^{(0)}(z)=\sum_{i=0}^{n} a_i(z-E_i)\ln(z-E_i), \tag{2.15}$$

can generate just such a linear interpolation of $\rho^{(0)}$ through

$$\rho^{(0)}(E)=-\pi^{-1}\,\mathrm{Im}[F^{(0)}(E+i0)]. \tag{2.5}$$

In determining the coefficients a_i needed to do this, we take the conventional definition of the principal value of $\ln(z)$:

$$\begin{aligned}&\mathrm{Im}\ln(E+i0)=\pi i, \quad E<0\\ &\mathrm{Im}\ln(E+i0)=0, \quad E>0\end{aligned} \tag{A3}$$

and put a branch cut along the negative real axis.

To fix the a_i, we compare $\rho^{(0)}(E)$ as given by (A1) and via (2.5) by (2.15) in each of the intervals (E_{i-1}, E_i). Matching the two expressions for E in the interval (E_{n-1}, E_n) determines a_n directly:

$$a_n=-b_n, \tag{A4}$$

while comparison in the interval (E_{j-1}, E_j) relates a_j to b_j and all the $a_{j+1},\ldots, a_n$. Let us assume that by induction we have determined the $a_{j+1},\ldots, a_n$, and seek a_j. Then, for E in (E_{j-1}, E_j), (2.15) and (2.5) imply

$$\rho^{(0)}(E)=-\sum_{i=j}^{n} a_i(E-E_i). \tag{A5}$$

Because we have already fixed $a_{j+1},\ldots, a_n$, (A5) becomes

$$\rho^{(0)}(E)=-a_j(E-E_j)+\rho_{j+1}+b_{j+1}(E-E_{j+1}). \tag{A6}$$

However, from (A1),

$$\rho^{(0)}(E)=\rho_j+b_j(E-E_j). \tag{A7}$$

Comparing (A7) with (A6) and using (A2) yields the general result

$$a_j=b_{j+1}-b_j. \tag{A8}$$

It remains to be shown that $F^{(0)}(z)\to 0$ as $1/z$ when $z\to\infty$ as required by the definition (2.14) and the asymptotic properties of $G^{(0)}$. Expanding the arguments of the natural logarithms in (2.15) in this limit in powers of z^{-1} yields

$$F^{(0)}(z)=\sum_{i=0}^{n} a_i(\ln z-E_i\ln z+E_i+0(z^{-1})), \tag{A9}$$

as $|z|\to\infty$. The coefficient of the $z\ln z$ term vanishes because, using (A8),

$$\sum_{i=0}^{n} a_i=\sum_{i=0}^{n}(b_{i+1}-b_i)=0. \tag{A10}$$

The coefficient $\sum_i a_iE_i$ can be evaluated by a summation by parts:

$$\begin{aligned}\sum_{i=0}^{n} a_iE_i=\sum_{i=0}^{n}(b_{i+1}-b_i)E_i=\sum_{i=0}^{n}(b_{i+1}E_{i+1}-b_iE_i)\\ -\sum_{i=0}^{n} b_{i+1}(E_{i+1}-E_i),\end{aligned} \tag{A11}$$

in which E_{n+1} is some arbitrary energy. The first term in the second line of (A11) vanishes because $b_{n+1}=b_0=0$, while the second term becomes, by (A1),

$$-\sum_{i=0}^{n} b_{i+1}(E_{i+1}-E_i)=\sum_{i=0}^{n}\rho_{i+1}-\rho_i=0, \tag{A12}$$

assuring the proper asymptotic behavior.

APPENDIX B: LOCALIZATION THEOREMS

Limitations on the configuration average of the spectrum of our model Hamiltonian may be obtained from two directions. Lifshitz[7] has argued intuitively that any eigenvalue of a pure crystal of either component will also be an eigenvalue of some configuration of the binary alloy. He reasons that in a random alloy there will be a nonvanishing probability of a sufficiently large cluster of like atoms to yield eigenenergies arbitrarily close to those of the pure substance. The spectrum of a pure A crystal, in our model, occupies the closed interval $(+\frac{1}{2}\delta+E_{\min}, \frac{1}{2}\delta+E_{\max})$, while the spectrum of a pure B crystal fills the interval $(-\frac{1}{2}\delta+E_{\min}, -\frac{1}{2}\delta+E_{\max})$. The conjecture of Lifshitz, therefore, is that the union of these two intervals must be contained within the averaged spectrum of any substitutional AB alloy.

In the rather special case of a one-dimensional alloy with certain restrictions on the atomic potentials, this conjecture can be proved, using mathematical tech-

niques which do no generalize to three dimensions.[27] We know of no proof for three dimesnions.

It can be shown rigorously for a very general clsas of alloy Hamiltonians, including the present, that there will be no states in the alloy with energies outside the limits just suggested. The proof uses methods developed by Kato,[28] applicable to any Hamiltonian constructed from bounded operators.

The two parts of our Hamiltonian (1.1), D and W, may be represented as bounded operators in a Hilbert space, in the sense that both have finite norm. We define, for convenience, the norm of an operator to be the magnitude of its largest eigenvalue. We now consider the operator $D+\lambda W$, where λ ranges from 0 to 1, and construct its resolvent:

$$R(z)\equiv(z-D-\lambda W)^{-1}. \tag{B1}$$

$R(z)$ has poles at all points in the spectrum of $D+\lambda W$, but is analytic elsewhere. The power-series expansion for $R(z)$,

$$R(z)=(z-D)^{-1}+(z-D)^{-1}\lambda W(z-D)^{-1} + (z-D)^{-1}\lambda W(z-D)^{-1}\lambda W(z-D)^{-1}+\ldots, \tag{B2}$$

converges absolutely for values of z such that

$$\lambda\|(z-D)^{-1}W\|\leqslant\lambda\|(z-D)^{-1}\|\,\|W\|<1. \tag{B3}$$

Of course, the convergence of the expansion in a region of z guarantees that no eigenvalues of $D+\lambda W$ lie in that region.

Since D has only two eigenvalues, $\frac{1}{2}\pm\delta$, the norm of $(z-D)^{-1}$ is simply the inverse of the distance between the point z and the nearest of $\pm\frac{1}{2}\delta$. The eigenvalues of W lie on the real axis, in the closed interval $(E_{\min}, E_{\max})$. If we assume that $E_{\max}=-E_{\min}$, then $\|W\|=E_{\max}$, and the series (B2) converges outside of two circles of radius $\lambda E_{\max}$, centered on $\pm\frac{1}{2}\delta$. This implies that the eigenvalues of $D+\lambda W$, which are real, must all be contained in the union of the intervals $(\frac{1}{2}\delta+\lambda E_{\min}, \frac{1}{2}\delta+\lambda E_{\max})$ and $(-\frac{1}{2}\delta+\lambda E_{\min}, -\frac{1}{2}\delta+\lambda E_{\max})$.

Setting $\lambda=1$ gives the limit sought for the spectrum of the model Hamiltonian. There is also a useful corollary. For $\lambda=0$, there will be exactly xN eigenstates of D with eigenvalue $\frac{1}{2}\delta$, and yN eigenstates with eigenvalue $-\frac{1}{2}\delta$. Since the eigenvalues are continuous functions of the parameter λ, there will be the same numbers of eigenstates of $D+\lambda W$ in the intervals $(\pm\frac{1}{2}\delta+E_{\min}, \pm\frac{1}{2}\delta+\lambda E_{\max})$ as there had been eigenstates of D at $\pm\frac{1}{2}\delta$, until the two intervals overlap. If δ is sufficiently large, $\delta>2$, that the two regions remain distinct when $\lambda=1$, there must be two separated sub-bands, which will contain xN and yN states apiece.

We assumed above that $E_{\max}$ and $|E_{\min}|$ were equal. It is trivial to remove this restriction by adding to W a constant ϕ,

$$\phi=-\tfrac{1}{2}(E_{\max}-E_{\min}), \tag{B4}$$

subtracting ϕ from D, and considering the resolvent

$$R_\phi(z)=[z-(D-\phi)-\lambda(W+\phi)]^{-1}. \tag{B5}$$

The norm of $W+\phi$ is $(E_{\max}-E_{\min})$, and the poles of (B5) lie in the intervals

$$(\pm\tfrac{1}{2}\delta+\tfrac{1}{2}(\lambda+1)E_{\min}-\tfrac{1}{2}(\lambda-1)E_{\max}, \pm\tfrac{1}{2}\delta+\tfrac{1}{2}(\lambda+1)E_{\max} -\tfrac{1}{2}(\lambda-1)E_{\min}).$$

For $\lambda=1$, this gives the same limits obtained above.

[27] J. M. Luttinger, Phillips Res. Rept. 6, 303 (1951).

[28] T. Kato, Progr. Theoret. Phys. (Kyoto) 4, 154 (1949), cited and discussed in A. Messiah, *Quantum Mechanics* (John Wiley & Sons, Inc., New York, 1962), p. 712ff.